AJNR

Differentiation of Low-Grade Oligodendrogliomas from Low-Grade Astrocytomas by Using Quantitative Blood-Volume Measurements Derived from Dynamic Susceptibility Contrast-Enhanced MR Imaging

Soonmee Cha, Tarik Tihan, Forrest Crawford, Nancy J. Fischbein, Susan Chang, Andrew Bollen, Sarah J. Nelson, Michael Prados, Mitchel S. Berger and William P. Dillon

AJNR Am J Neuroradiol 2005, 26 (2) 266-273
http://www.ajnr.org/content/26/2/266

AJNR Am J Neuroradiol 26:266–273, February 2005

Differentiation of Low-Grade Oligodendrogliomas from Low-Grade Astrocytomas by Using Quantitative Blood-Volume Measurements Derived from Dynamic Susceptibility Contrast-Enhanced MR Imaging

Soonmee Cha, Tarik Tihan, Forrest Crawford, Nancy J. Fischbein, Susan Chang, Andrew Bollen, Sarah J. Nelson, Michael Prados, Mitchel S. Berger, and William P. Dillon

BACKGROUND AND PURPOSE: **Histopathologic evaluation remains the reference standard for diagnosis of glioma and classification of histologic subtypes, but is challenged by subjective criteria, tissue sampling error, and lack of specific tumor markers. Anatomic imaging is essential for surgical planning of gliomas but is limited by its nonspecificity and its inability to depict beyond morphologic aberrations. The purpose of our study was to investigate dynamic susceptibility contrast-enhanced (DSC) MR imaging characteristics of the two most common subtypes of low-grade infiltrating glioma: astrocytoma and oligodendroglioma. We hypothesized that tumor blood-volume measurements, derived from DSC MR imaging, would help differentiate the two on the basis of differences in tumor vascularity.**

METHODS: **We studied 25 consecutive patients with treatment-naïve, histopathologically confirmed World Health Organization grade II astrocytoma ($n = 11$) or oligodendroglioma ($n = 14$). All patients underwent anatomic and DSC MR imaging immediately before surgical resection. Histologic confirmation was obtained in all patients. Anatomic MR images were analyzed for morphologic features, and DSC MR data were processed to yield quantitative cerebral blood volume (CBV) measurements.**

RESULTS: **The maximum relative CBV ($rCBV_{max}$) in tumor ranged from 0.48 to 1.34 (0.92 ± 0.27, median ± SD) in astrocytomas and from 1.29 to 9.24 (3.68 ± 2.39) in oligodendrogliomas. The difference in median $rCBV_{max}$ between the two tumor types was significant ($P < .0001$).**

CONCLUSION: **The tumor $rCBV_{max}$ measurements derived from DSC MR imaging were significantly higher in low-grade oligodendrogliomas than in astrocytomas. Our findings suggest that tumor $rCBV_{max}$ derived from DSC MR imaging can be used to distinguish between the two low-grade gliomas.**

Low-grade infiltrating gliomas comprise a heterogeneous group of slow-growing tumors, and the two most common histologic subtypes are astrocytoma and oligodendroglioma (1). Although histopathologic evaluation remains the reference standard for the diagnosis and histologic subtyping of low-grade gliomas, it is limited by issues such as subjective criteria, tissue sampling error, and lack of any specific tumor marker (2, 3).

Anatomy-based MR imaging with intravenous contrast material is the accepted standard for preoperative localization and characterization of brain tumor. Despite its exquisite sensitivity in tumor detection, anatomic MR imaging is not sufficiently specific enough to permit a confident differentiation between various grades and subtypes of gliomas. Recent progress in physiology-based dynamic MR imaging methods, however, promises to improve specificity and provide insight into the underlying biologic characteristics of brain tumors (4).

Received November 14, 2003; accepted after revision May 10, 2004.

From the Departments of Radiology (S. Cha, F.C., N.J.F., S.J.N., W.P.D.), Neurological Surgery (S. Cha, S. Chang, M.P., M.S.B., W.P.D.), and Pathology (T.T., A.B.), University of California San Francisco Medical Center.

Supported by National Institute of Neurological Disorders and Stroke (K23 NS45013) and Accelerate Brain Cancer Cure, Inc.

Address reprint requests to Soonmee Cha, MD, Department of Radiology, Box 0628, UCSF Medical Center, 505 Parnassus Ave, Rm L358, San Francisco, CA 94143-0628

No longer simply a research tool, dynamic susceptibility-weighted contrast-enhanced (DSC) MR imaging is now used clinically to noninvasively assess tumor vascularity. DSC MR imaging-derived relative cerebral blood volume (rCBV) measurements have been shown to correlate with glioma grade and conventional angiographic vascularity, and indirectly with tumor angiogenesis and biologic aggressiveness (5–8). A recently published report by Lev et al (9) suggests, however, that glioma grading based on rCBV measurements can be affected by the inclusion of oligodendrogliomas. The purpose of our study was to investigate DSC MR imaging characteristics of the two most common subtypes of low-grade infiltrating glioma—astrocytoma and oligodendroglioma—to test the hypothesis that tumor blood-volume measurements derived from DSC MR imaging would differentiate the two on the basis of differences in tumor vascularity.

Methods

Subjects

From June 2002 to December 2003, we studied 25 consecutive patients with treatment-naïve, histopathologically confirmed World Health Organization (WHO) grade II astrocytomas (n = 11) or grade II oligodendrogliomas (n = 14). Of those patients with grade II oligodendrogliomas, five were women and nine were men (age range, 19–65 years; mean, 44.5 years). Of those with grade II astrocytomas, six were women and five were men (age range, 22–68 years; mean, 27 years). All patients were studied before receiving any treatment and immediately before surgery. All patients had frameless head fiducials in place for intraoperative localization and underwent MR imaging with use of a 1.5-T magnet (Signa Horizon Lx Echospeed; GE Medical Systems, Milwaukee, WI). Informed consent for participation in this study was obtained from each patient by using a protocol approved by our institutional review board.

Histologic Analysis

All tissues obtained from surgical resections, including cavitron ultrasonic aspiration material, were subjected to routine processing and histologic analysis with hematoxylin-eosin staining. The tumors were classified and graded according to the current WHO criteria (10). High-grade tumors, as well as low-grade mixed gliomas (tumors that contained classic biphasic oligoastrocytomas), were excluded from the study. Two neuropathologists (A.B., T.T.) separately reviewed all the slides from each patient without knowledge of the imaging or clinical data.

Immunohistochemistry

In all 25 patients, parallel sections from paraffin-embedded tissue blocks were obtained for histochemical and immunohistochemical analysis. Immunohistochemistry was performed by using the standard streptavidin-biotin technique with appropriate negative and positive controls. Monoclonal antibody MIB-1 antibody (dilution 1:150; Immunotech, Marseilles, France) was used to determine the proliferation index. The proliferation index was determined by counting approximately 1000 tumor cells where the nuclear positivity was highest within the tumors. CD31 antibody (monoclonal, dilution 1:100; DAKO, Carpinteria, CA) was used for qualitative assessment of microvascular density for all tumor specimens. The microvascular density was then evaluated against the vascular density of the normal brain and then comparatively recorded as "high" or "low."

MR Imaging

All patients underwent the same preoperative MR imaging protocol, which consisted of a three-plane localizer sequence (8.5/1.6 ms [TR/TE]), an axial fluid-attenuated inversion-recovery (FLAIR) sequence (10,000/148/2200 [TR/TE/TI]), an axial fast spin-echo T2-weighted sequence (3000/102, echo train length 16, matrix 256 × 196), axial diffusion-weighted imaging (10,000/99, b = 1000 s/mm^2), dynamic contrast-enhanced gradient-echo echo-planar imaging (1250/54, flip angle 30°), and a postcontrast 3D spoiled gradient-recalled acquisition in the steady state ([SPGR] 34/8) T1-weighted sequence.

For dynamic echo-planar imaging, the location and size of the tumor and the position of the superior and inferior margins were determined from the T2-weighted and FLAIR images. Seven to eight sections, 3–5 mm thick (gap, 0–2 mm), were selected to contain the entire tumor volume. The first five image sets were obtained before injection of the contrast agent to establish a precontrast baseline. A standard dose of the paramagnetic contrast agent gadopentetate dimeglumine (0.1 mmol/kg body weight; Omniscan; Amersham Health, Castro Valley, CA) was injected intravenously with an MR-compatible power injector at a rate of 4 or 5 mL/s through an antecubital angiocatheter (18–21 gauge), followed immediately by a 20-mL continuous saline flush. The multisection image set was acquired at a rate of one image per section per second for a total of 60 seconds.

Anatomic Image Analysis

Two neuroradiologists (N.J.F., W.P.D.) reviewed each tumor for the following imaging characteristics: contrast enhancement, intratumoral cyst, tumor border, T2 signal intensity characteristics of the tumor, and intratumoral susceptibility (defined as hypointense signal abnormality) on precontrast gradient-echo images. The two neuroradiologists were blinded to the histopathologic diagnosis and grade. Based on the anatomic MR imaging characteristics, the two readers were asked to decide whether the tumor was an oligodendroglioma or an astrocytoma and to determine the tumor grade based on the WHO glioma grading classification. Each tumor was assessed for presence or absence of contrast enhancement on T1-weighted images and, when present, the enhancing portion of the tumor was estimated as a percentage of the nonenhancing tumor volume.

Image Processing

Image postprocessing was performed by using software programs written in C, Fortran, MATLAB, and IDL programming languages. During the first pass of the gadolinium-based contrast bolus, signal intensity decreases on T2*-weighted images. Relative concentration of the contrast material can be calculated from signal intensity changes to obtain a plot of the relative concentration of contrast material in tissue over time. The area under this curve is proportional to the regional CBV. Correction for contrast material recirculation and leakage (which invalidates the CBV calculation) was performed by subtracting a baseline T2* susceptibility signal intensity from under the contrast agent bolus. The beginning and end of the bolus passage were defined as the images at which the signal intensity came within 1 SD of the mean pre- and post-bolus signal intensities, respectively. The end of the first pass was estimated by using gamma-variate fitting to eliminate arbitrary criteria.

The raw T2*-weighted echo-planar data were transferred to a UNIX workstation (Sunblade 100; Sun Computer, Mountain View, CA) for off-line postprocessing. The dynamic T2*-weighted image postprocessing was performed with a software written in C programming language, yielding a gray-scale rCBV map by using the method described above. The postcontrast 3D SPGR T1-weighted images, the rCBV maps, and the first time point acquisition of the T2*-weighted echo-planar image were

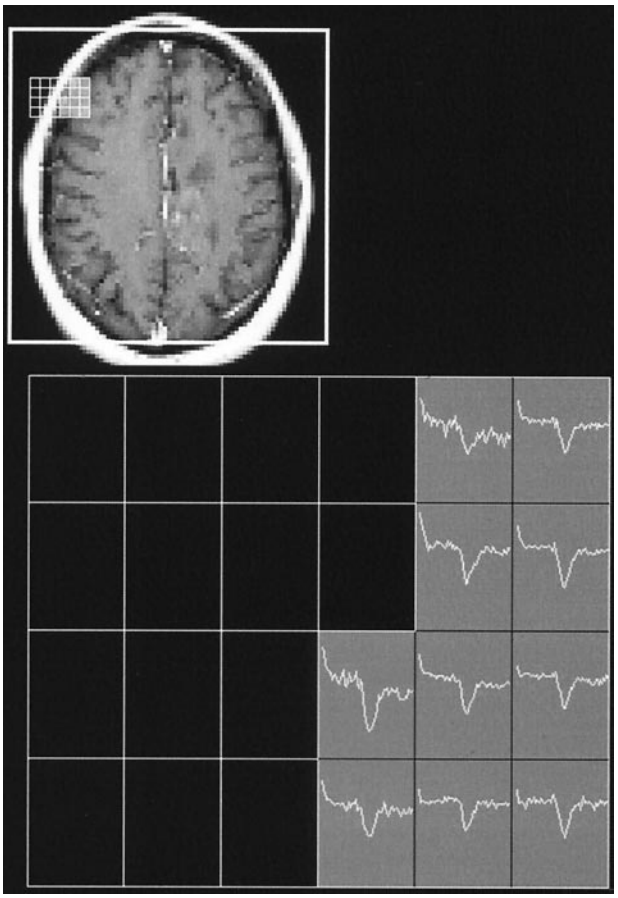

FIG 1. T2* signal intensity time curves from normal cortical and background ROIs.

then imported into a volume file developed in-house for the purpose of artifact elimination and resampling. Figure 1 demonstrates T2* signal intensity time curves from the normal cortical and the background regions of interest (ROIs).

For quantification of blood volume, tumor CBV was expressed as rCBV, where r indicates *relative,* meaning compared with an internal reference, which in this study was the normal contralateral white matter. To improve the signal-to-noise ratio in the measurements, rCBV values were then calculated in ROIs in the areas that showed the greatest values on gray-scale maps. Each ROI measured 5 mm for all tumors. The ROIs were chosen on the basis of automated analysis of T2* signal intensity curve characteristics that showed maximum amplitude of signal intensity decrease during the first pass and rCBV maps generated pixel-by-pixel. In each tumor, four or five ROIs were chosen in the contrast enhancing (if present) as well as the nonenhancing portion of the tumor to obtain the maximum rCBV ($rCBV_{max}$).

Statistical Analyses

Because of the small patient sample and non-normal distribution of continuous variables, nonparametric statistics were used. The Fisher exact test was performed to determine the difference in anatomic imaging variables (e.g., frontal lobe location, intratumoral cyst, cortical involvement, tumor border, and susceptibility) between low-grade oligodendrogliomas and low-grade astrocytomas. The Wilcoxon rank sum test was used for analysis of age, tumoral enhancement, $rCBV_{max}$, and MIB-1 labeling index. The Spearman rank coefficient was obtained to determine the correlation between age and rCBV, and age and MIB-1 labeling index. Analysis of covariance (ANCOVA) was used to adjust for age and to determine differences between the two tumor types. Least squares means and 95% confidence intervals (CIs) were used to describe the group differences in ANCOVA analysis. *P* values of ANCOVA were determined by using ranks of the dependent variables in the ANCOVA. A *P* value of .05 or less was considered to indicate a statistically significant difference.

Results

Histopathologic Characteristics

Histologic confirmation was made from resected tissue specimens in all 25 patients. None of the patients underwent biopsy only for histologic diagnosis. Low-grade astrocytomas demonstrated typical diffuse involvement by hyperchromatic and moderately pleomorphic tumor cells imperceptively admixed with the underlying neural parenchyma without mitotic figures, vascular proliferation, or necrosis. In some cases, focal microcystic change was present. In none of these tumors was an oligodendroglial component perceived.

Low-grade oligodendrogliomas were composed of highly monotonous tumor cells and characteristically displayed "chicken-wire" type of hypervascularity. Most tumors involved the cortex, with typical satellitosis, nuclear chains, and subpial crowding. No appreciable astrocytic component was noted in any of these tumors.

The two neuropathologists who independently reviewed the histologic slides in all 25 patients confirmed that none of the tumors were classic mixed oligoastrocytomas and none met the criteria for WHO grade III anaplastic oligodendroglioma or astrocytoma.

Immunohistochemical Analysis

Paraffin tissue blocks were available in all 25 tumor specimens for immunohistochemical analysis. The MIB-1 labeling index in the immunohistochemical assessment of the proliferation index of tumor tissue samples ranged as follows: 0.50–10.94% (mean ± SD, 3.16 ± 3.42%) for the 14 low-grade oligodendrogliomas and 1.11–8.34% (mean ± SD, 3.75 ± 2.82%) for the 11 low-grade astrocytomas. The difference in the mean MIB-1 labeling indexes between the two tumor types was not statistically significant ($P = .1015$). These data are displayed in Figure 2. Likewise, the difference in the median MIB-1 labeling indexes between oligodendrogliomas and astrocytomas was not significant (1.9% vs. 2.0%, respectively, $P = .4933$ Wilcoxon rank sum test).

Qualitative analysis of tumor vascularity by using CD31 immunohistochemistry as well as routine stains demonstrated an overall increase in vascularity among the oligodendrogliomas compared with the astrocytomas. The vascular density did not appear to differ from normal brain vasculature for grade II astrocytomas. However, a distinct increase was evident in the delicate capillary vessels in almost all oligodendrogliomas, which was partly responsible for the chicken-wire appearance of the tumor (Fig 3).

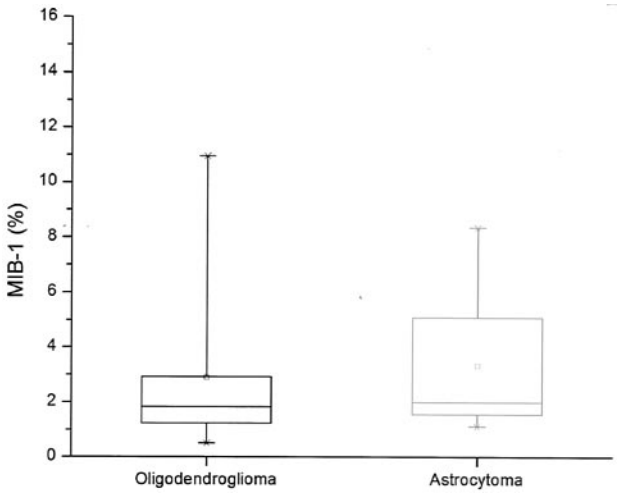

FIG 2. Box plot of mitotic index labeling (MIB-1) for each tumor shows similar mean values, indicated by the small squares for both tumor types, with a larger SD for low-grade astrocytoma. Horizontal line in box indicates median.

Anatomic MR Images

The anatomic MR imaging characteristics of the two tumor types in our study were similar to what has been published before. Except for cortical involvement, no other anatomic imaging feature or combination of features would permit any confident differentiation between the tumor types. Oligodendrogliomas more commonly displayed enhancement, a frontal-lobe location, cortical involvement, the presence of intratumoral cysts, and susceptibility. Representative images of the oligodendroglioma and astrocytoma are shown in Figures 4 and 5, respectively. In the blinded assessment of anatomic imaging features, each of the two neuroradiologists considered the presence of intratumoral cysts, susceptibility, and cortical involvement to be the most likely anatomic MR imaging features to be predictive of oligodendroglioma. When using the anatomic criteria, these readers correctly predicted the histologic tumor type in nine (64%) of the 14 oligodendrogliomas and eight (72%) of the 11 astrocytomas. Based on results of the Fisher exact test, only cortical involvement of tumor reached statistical significance ($P = .0486$), whereas all other anatomic imaging features did not.

DSC MR Imaging

The $rCBV_{max}$ of tumors ranged from 0.48 to 1.34 (median ± SD, 0.92 ± 0.27) for astrocytomas and from 1.29 to 9.24 (median ± SD, 3.68 ± 2.39) in oligodendrogliomas (Fig 6). The difference in median $rCBV_{max}$ values between the two tumor types was significant ($P < .0001$) by using the Wilcoxon rank sum test and ANCOVA. The least squares mean for $rCBV_{max}$ after adjustment for age was 0.7357 (95% CI: 0.4170–1.8884) in astrocytomas and 4.2841 (95% CI: 3.2696–5.2985) in oligodendrogliomas. After adjustment for age, the difference in $rCBV_{max}$ between the two tumor types was still significant ($P = .0001$) by using ANCOVA.

The $rCBV_{max}$ measurements varied greatly within each individual oligodendroglioma, whereas the astrocytomas tended to have little, if any, variation in $rCBV_{max}$ within each individual tumor. All of the astrocytomas had $rCBV_{max}$ values of less than 1.5 when compared with the contralateral normal white matter, as opposed to only one of the 14 oligodendrogliomas.

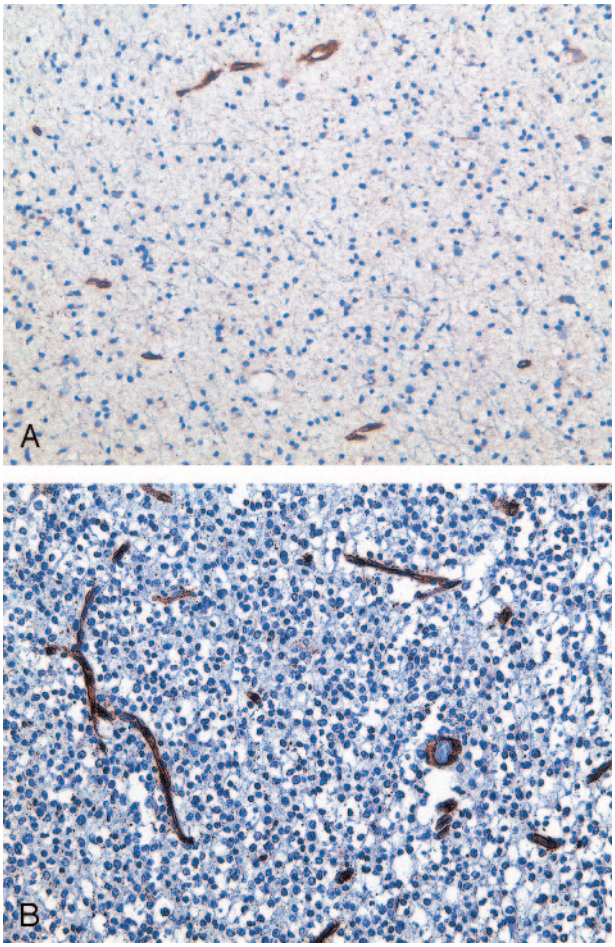

FIG 3. *A* and *B*, Photomicrographs from immunohistochemistry of endothelial cell marker (CD31) in low-grade gliomas (CD31 stain; original magnification, X400). Grade II astrocytoma (*A*) shows minimal reactivity with CD31 antibody compared with a grade II oligogdendroglioma (*B*), which demonstrates strong reactivity as shown by the brown staining of the vasculature.

Statistical Analysis

The Fisher exact test for each anatomic imaging variable (e.g., frontal lobe location, intratumoral cyst, cortical involvement) revealed no statistically significant differences, except in cortical involvement. Wilcoxon rank sum test for analysis of age, percentage of tumoral enhancement, $rCBV_{max}$, and MIB-1 labeling index also showed no statistically significant differences, except in $rCBV_{max}$. Spearman rank coefficient showed no correlation between age and $rCBV_{max}$ or age and MIB-1 labeling index. ANCOVA was used to adjust for age, and there was still a significant difference in $rCBV_{max}$ between the two tumor types ($P = .0001$).

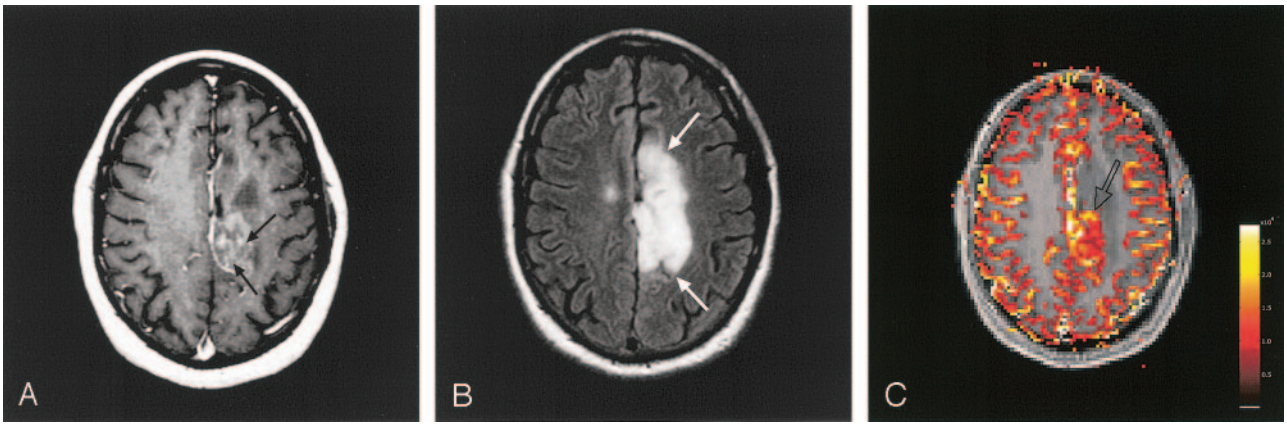

FIG 4. Case of a 40-year-old man with a grade II oligodendroglioma.
A and *B*, Axial contrast-enhanced T1-weighted (*A*) and FLAIR (*B*) MR images demonstrate a heterogeneously enhancing (black arrows), infiltrative, cortically based mass (white arrows) in the left medial superior frontal lobe.
C, Relative CBV map of the tumor shows a large focus of increased blood volume (arrow) in the tumor.

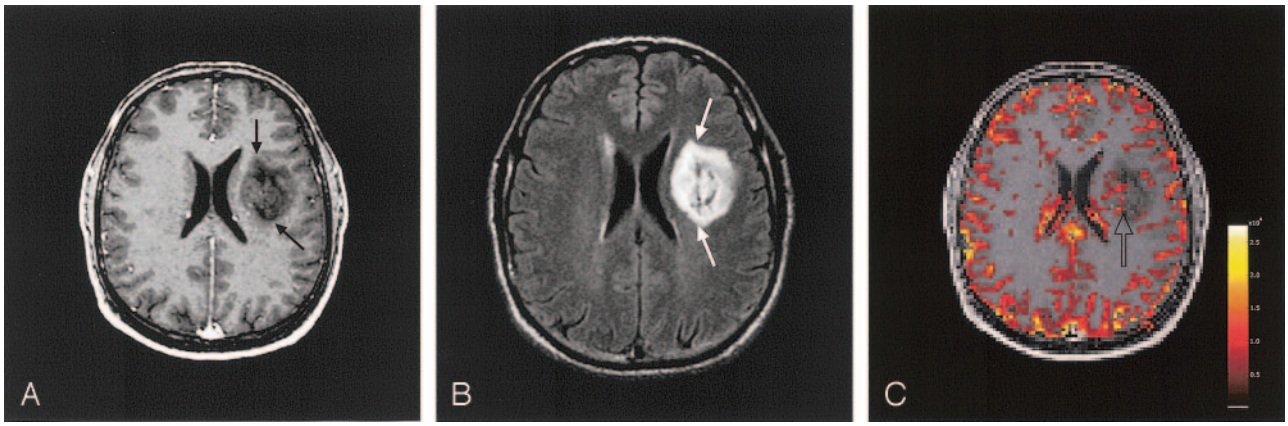

FIG 5. Case of a 32-year-old man with a grade II astrocytoma.
A and *B*, Axial contrast-enhanced T1-weighted (*A*) and FLAIR (*B*) MR images demonstrate a minimally enhancing (black arrows), heterogeneous T2 hyperintense mass (white arrows) in the left deep frontal white matter.
C, Relative CBV map of the tumor shows minimally elevated blood volume in the tumor (arrow).

Discussion

Differentiating low-grade astrocytomas from low-grade oligodendrogliomas preoperatively with use of imaging is important for several reasons. First, these two tumor types are well-defined, clinicopathologic entities with distinct biologic and prognostic characteristics for which distinction based on histopathologic evaluation, the current reference standard, can be difficult and not without error (2, 3, 11). The histopathologic evaluation of low-grade glioma is challenged by a mixed cellular component in a given tumor that can lead to subjective criteria for determining the cell of origin, inherent sampling error associated with a surgical tissue specimen, and lack of specific tumor markers. Preoperative anatomic imaging already plays a complementary role by providing information on tumor location, surgical resectablity, satellite focus of tumor, and reactive changes in the adjacent brain—all of which are important factors influencing treatment and outcome, but which cannot be assessed directly from histopathologic evaluation.

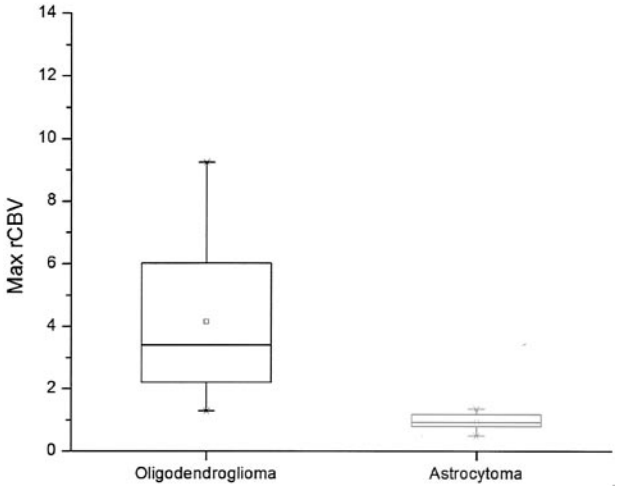

FIG 6. Box plot of $rCBV_{max}$ for each tumor shows a significant difference in mean $rCBV_{max}$ values (small squares) between low-grade oligodendroglioma and low-grade astrocytoma, with a larger SD for low-grade oligodendroglioma. Horizontal line in box indicates median.

Nevertheless, anatomic MR imaging suffers from nonspecifity and the inability to depict beyond morphologic aberration. With the addition of nonanatomic, physiology-based MR imaging methods such as perfusion MR imaging, however, more sophisticated tumor characterization that can provide insight into the underlying biologic characteristics is now possible. Thus, it is critical to define preoperatively the physiologic MR imaging features of well-defined tumor types, at their native state, to complete imaging characterization. A great step forward would be if the challenges presented by patients with glioma could be more accurately predicted *before* the surgical approach, thus directing tissue specimens for appropriate histologic and molecular analysis, as well as empowering the radiation and neuro-oncology colleagues with better assessment of treatment choices and prognosis.

Second, although not yet widely available, therapies such as convection-enhanced drug delivery are being developed for the purpose of preoperative or intraoperative use in gliomas (12–14). Knowing the likelihood of tumor histologic subtype would be of critical importance in planning such therapies. With the current traditional therapy for gliomas being far from successful (15) and with progress occurring in innovative but risky targeted interventions, preoperative anatomic and physiologic imaging of gliomas at their native state to assess biologic subtypes, vascularity, and other physiologic parameters will be not only mandatory but also unavoidable in the near future.

Third, similar to the advances in imaging, impressive developments have occurred in tumor genetics that promise to unravel molecular and chromosomal aberrations in gliomas (16–20), which could potentially revolutionize how these tumors are diagnosed and treated. Molecular biology of gliomas, however, suffers from similar constraints as those of histopathology in that the evaluation is limited to the tissue at hand, and hence, the whole tumor cannot be evaluated. It also ignores other important prognostic factors such as biologic characteristics of residual tumor. Furthermore, because of the limited availability and high cost of the necessary elaborate laboratory systems, performing tumor genetics on a routine basis is not yet a reality. Hence, if imaging can stratify preoperatively which tumor subtypes should undergo further molecular and genetic analysis, such as 1p and 19q alleic chromosomal losses in oligodendroglioma (21), this could potentially alter postoperative therapy, help assess prognosis, and offer great benefit to the patient.

In the current study, we evaluated perfusion MR imaging characteristics in two well-defined clinicopathologic glioma subtypes and found that low-grade astrocytomas and oligodendrogliomas have significantly different tumor blood-volume measurements. This is in keeping with numerous published reports on the difference in histologic evidence of differential vascularity between these two tumor types. The difference in MR imaging–derived tumor blood-volume measurements between oligodendrogliomas and astrocytomas may be due to a lack of neoangiogenesis or vascular proliferation in astrocystomas and the presence of capillary neovascularization in oligodendrogliomas. Alternatively, higher rCBV in oligodendrogliomas may, in part but not exclusively, be related to their cortical location. Because the normal cortical gray matter contains a greater number of blood vessels compared with that of white matter, tumors involving the gray matter may have higher vascular density. Since the tumor $rCBV_{max}$ was expressed as a ratio to the contralateral white matter, the higher blood volume of oligodendrogliomas may in part be attributed to their higher likelihood of cortical involvement. Mineura et al (22) reported on fluorodeoxyglucose positron emission tomographic (PET) features of five grade II oligodendrogliomas in which they found a decrease in tumor blood volume and flow. This apparent discrepancy in rCBV between PET and DSC MR imaging may, in part, be explained by the fact that they used contralateral gray matter as the internal reference, whereas we used white matter. Nevertheless, as shown in Figure 7, most of our cortically based oligodendrogliomas had increased blood volume even when compared with the contralateral normal gray matter. Our histologic evaluation showed clear evidence of neovascularization in oligodendrogliomas that was distinct from what one would expect as a normal increase in gray matter vasculature, thus suggesting that the rCBV derived from DSC MR imaging better correlates with histopathologic findings than does rCBV derived from PET.

Several studies have shown that oligodendrogliomas express powerful proangiogenic mitogens, such as vascular endothelial growth factor (23–25) and hypoxia-inducible factor-1α (26), that contribute to their neovascularization and vascular hyperplasia. Schiffer et al (27, 28) also have described the unique vascularity of oligodendrogliomas, in which increased vascular density was seen in both low-grade and high-grade oligodendrogliomas. That pattern was in contrast to the pattern in fibrillary astrocytomas, for which microvascular proliferation was seen in only the higher-grade tumors. Our findings indicate that MR imaging -derived tumor blood-volume measurements reflect the degree of tumor angiogenesis and correlate with histologic differences in tumor vasculature between low-grade oligodendrogliomas and astrocytomas.

Our study results also suggest that low-grade oligodendrogliomas are more vascular than astrocytomas at both histologic evaluation and perfusion MR imaging. This finding corroborates with results of a recent study published by Lev et al (9) that glioma grading based on MR-derived rCBV measurements may not be accurate if low-grade oligodendroglioma is included in the sample.

Our findings that show relatively high tumor blood-volume values associated with grade II oligodendrogliomas have an important implication in glioma grading based on rCBV measurements. Several studies (5–7) reported a positive correlation between glioma grade and rCBV values, wherein the glioma

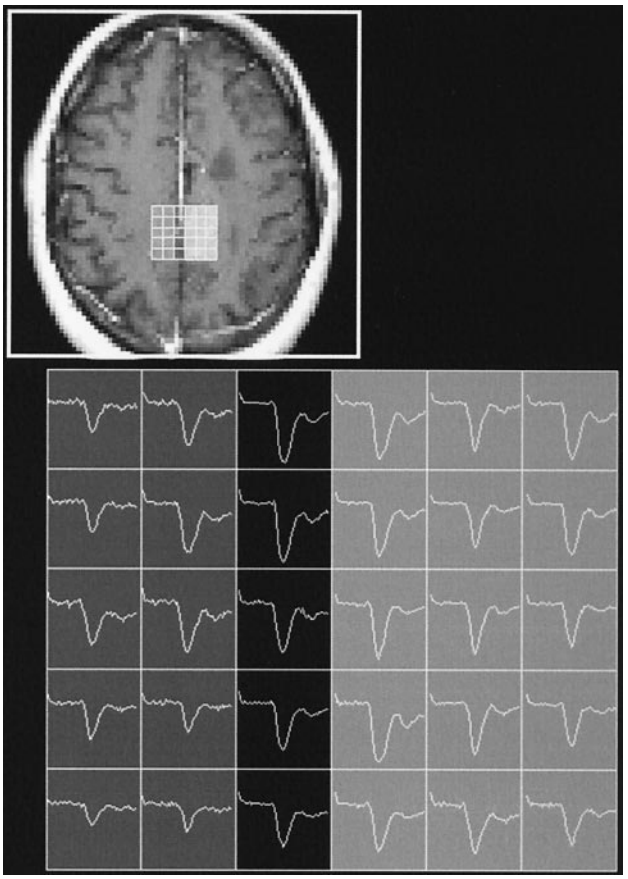

FIG 7. Multiple voxels of T2* signal intensity time curves in a left superior frontal oligodendroglioma (same patient as in Fig 4) demonstrate more pronounced signal intensity decrease within the tumor (lighter shaded area) when compared with the contralateral gray matter (darker shaded area).

group consisted solely of astrocytomas (6) or the glioma subtypes were not specified in the study (5, 7). Our results suggest that rCBV-based grading of gliomas as a general class may not show a positive correlation with histopathologic grading if low-grade oligodendrogliomas are included in the sample of gliomas. On that basis, we suggest that glioma grading based on MR imaging-derived rCBV measurements be limited to fibrillary astrocytomas only.

Our study results further suggest that among the well-established anatomic MR imaging features of oligodendrogliomas and astrocytomas, only involvement of the cortical gray matter was significantly correlated with low-grade oligodendroglioma ($P = .0486$). However, none of the individual anatomic features observed alone or in combination with another feature reached statistical significance. The imaging evidence of cortical involvement in oligodendrogliomas correlated well with our histopathologic findings of tumors extending into the cortex with typical satellitosis, nuclear chains, and subpial crowding.

The issue remains whether rCBV derived from DSC MR imaging can distinguish indolent from more malignant oligodendrogliomas. Correlative histopathologic and long-term outcome studies have reported conflicting results on the relationship between neovascularization and prognosis in patients with oligodendrogliomas. Prognostic value of histologic grading of oligodendroglial tumors remains controversial, and interobserver reproducibility in grading of these tumors is unknown (24, 26, 28, 29). It is widely accepted, however, that the neovascularization is commonly seen in low-grade oligodendrogliomas and that, unlike astrocytic tumors, endothelial hyperplasia alone is not a strong independent factor of unfavorable prognosis (28, 29). In our study, we did not evaluate any high-grade oligodendrogliomas simply because we did not have a sufficient number of these cases to include in the study. Since neovascularization is known to be present in both low- and high-grade oligodendrogliomas, and in and of itself is not essential in determining the grade of an oligodendroglioma, it is doubtful that rCBV derived from DSC MR imaging would be helpful in distinguishing different grades of this tumor type.

One of the major limitations of our study is the lack of a direct correlation between MR imaging-derived tumor blood volume and histologic correlate. We do not fully understand exactly what is responsible for an elevated blood volume in grade II oligodendrogliomas—whether it may be the distinct vascular pattern, the presence of capillaries, dilated vessels within the tumor, predominant cortical location, a combination of these factors, or some other yet unknown factors. Further investigations to directly correlate imaging with histologic standards will strengthen the validity of the MR imaging-derived blood-volume measurement as a noninvasive imaging marker of tumor angiogenesis.

As we move into an even more sophisticated clinical setting with advances in stereotactic surgical procedures, tumor immunohistochemistry and genetics, and noninvasive anatomic and physiologic imaging, it becomes inevitable to think that a real-time correlation among imaging, histopathologic, and molecular biologic characteristics of brain tumors is not only mandatory, but unavoidable. We believe that noninvasive imaging will play a much more substantive role in the preoperative diagnosis and management of brain tumors as we move toward higher field strength MR imaging and physiology-based imaging schemes, as well as unconventional therapeutic interventions before surgery.

Conclusion

The results of our study suggest that the measurement of tumor blood volume derived from DSC MR imaging yields information about the tumor vasculature and is useful in improving the specificity of the diagnosis of grade II oligodendrogliomas and grade II astrocytomas. Preoperative differentiation of oligodendroglioma and astrocytoma with use of noninvasive anatomic and physiologic imaging is important for establishing imaging as a second reference standard to histopathologic evaluation, empowering neurosurgeons and neuro-oncologists to plan for poten-

tial pre- or intraoperative therapy, and stratifying tissue specimens for appropriate molecular and genetic analyses that can guide therapy and help assess prognosis.

References

1. Lopes M, Laws EJ. **Low-grade central nervous system tumors**. *Neurosurg Focus* 2002;12:1–4
2. Sasaki H, Zlatescu MC, Betensky RA, et al. **Histopathological-molecular genetic correlations in referral pathologist-diagnosed low-grade "oligodendroglioma"**. *J Neuropathol Exp Neurol* 2002; 61:58–63
3. van den Bent M. **New perspectives for the diagnosis and treatment of oligodendroglioma**. *Expert Rev Anticancer Ther* 2001;1:348–356
4. Pomper MG, Port JD. **New techniques in MR imaging of brain tumors**. *Magn Reson Imaging Clin N Am* 2000;8:691–713
5. Aronen HJ, Gazit IE, Louis DN, et al. **Cerebral blood volume maps of gliomas: comparison with tumor grade and histologic findings**. *Radiology* 1994;191:41–51
6. Knopp EA, Cha S, Johnson G, et al. **Glial neoplasms: dynamic contrast-enhanced T2*-weighted MR imaging**. *Radiology* 1999;211: 791–798
7. Sugahara T, Korogi Y, Kochi M, et al. **Correlation of MR imaging-determined cerebral blood volume maps with histologic and angiographic determination of vascularity of gliomas**. *AJR Am J Roentgenol* 1998;171:1479–1486
8. Aronen HJ, Pardo FS, Kennedy DN, et al. **High microvascular blood volume is associated with high glucose uptake and tumor angiogenesis in human gliomas**. *Clin Cancer Res* 2000;6:2189–2200
9. Lev MH, Ozsunar Y, Henson JW, et al. **Glial tumor grading and outcome prediction using dynamic spin-echo MR susceptibility mapping compared with conventional contrast-enhanced MR: confounding effect of elevated rCBV of oligodendroglimoas**. *AJNR Am J Neuroradiol* 2004;25:214–221
10. Kleihues P, Sobin LH. **World Health Organization classification of tumors**. *Cancer* 2000;88:2887
11. Coons SW, Johnson PC, Scheithauer BW, Yates AJ, Pearl DK. **Improving diagnostic accuracy and interobserver concordance in the classification and grading of primary gliomas**. *Cancer* 1997; 79:1381–1393
12. Morrison PF, Chen MY, Chadwick RS, Lonser RR, Oldfield EH. **Focal delivery during direct infusion to brain: role of flow rate, catheter diameter, and tissue mechanics**. *Am J Physiol* 1999;277: R1218–1229
13. Groothuis DR. **The blood-brain and blood-tumor barriers: a review of strategies for increasing drug delivery**. *Neuro-oncol* 2000;2:45–59
14. Husain SR, Puri RK. **Interleukin-13 receptor-directed cytotoxin for malignant glioma therapy: from bench to bedside**. *J Neurooncol* 2003;65:37–48
15. Prados MD, Levin V. **Biology and treatment of malignant glioma**. *Semin Oncol* 2000;27:1–10
16. Wild-Bode C, Weller M, Wick W. **Molecular determinants of glioma cell migration and invasion**. *J Neurosurg* 2001;94:978–984
17. Smith JS, Jenkins RB. **Genetic alterations in adult diffuse glioma: occurrence, significance, and prognostic implications**. *Front Biosci* 2000;5:D213–231
18. Fathallah-Shaykh HM, Zhao LJ, Mickey B, Kafrouni AI. **Molecular advances to treat cancer of the brain**. *Expert Opin Investig Drugs* 2000;9:1207–1215
19. Cairncross JG, Ueki K, Zlatescu MC, et al. **Specific genetic predictors of chemotherapeutic response and survival in patients with anaplastic oligodendrogliomas**. *J Natl Cancer Inst* 1998;90:1473–1479
20. Bogler O, Huang HJ, Kleihues P, Cavenee WK. **The p53 gene and its role in human brain tumors**. *Glia* 1995;15:308–327
21. Smith JS, Perry A, Borell TJ, et al. **Alterations of chromosome arms 1p and 19q as predictors of survival in oligodendrogliomas, astrocytomas, and mixed oligoastrocytomas**. *J Clin Oncol* 2000;18:636–645
22. Mineura K, Shioya H, Kowada M, Ogawa T, Hatazawa J, Uemura K. **Blood flow and metabolism of oligodendrogliomas: a positron emission tomography study with kinetic analysis of 18F-fluorodeoxyglucose**. *J Neurooncol* 1999;43:49–57
23. Christov C, Gherardi RK. **Vascular endothelial growth factor (VEGF) likely contributes to oligodendroglioma angiogenesis**. *Acta Neuropathol (Berl)* 1999;97:429–432
24. Varlet P, Guillamo JS, Nataf F, Koziak M, Beuvon F, Daumas-Duport C. **Vascular endothelial growth factor expression in oligodendrogliomas: a correlative study with Sainte-Anne malignancy grade, growth fraction and patient survival**. *Neuropathol Appl Neurobiol* 2000;26:379–389
25. Christov C, Adle-Biassette H, Le Guerinel C, Natchev S, Gherardi RK. **Immunohistochemical detection of vascular endothelial growth factor (VEGF) in the vasculature of oligodendrogliomas**. *Neuropathol Appl Neurobiol* 1998;24:29–35
26. Birner P, Gatterbauer B, Oberhuber G, et al. **Expression of hypoxia-inducible factor-1 alpha in oligodendrogliomas: its impact on prognosis and on neoangiogenesis**. *Cancer* 2001;92:165–171
27. Schiffer D, Bosone I, Dutto A, Di Vito N, Chio A. **The prognostic role of vessel productive changes and vessel density in oligodendroglioma**. *J Neurooncol* 1999;44:99–107
28. Schiffer D, Dutto A, Cavalla P, et al. **Prognostic factors in oligodendroglioma**. *Can J Neurol Sci* 1997;24:313–319
29. Mork SJ, Halvorsen TB, Lindegaard KF, Eide GE. **Oligodendroglioma: histologic evaluation and prognosis**. *J Neuropathol Exp Neurol* 1986;45:65–78